The *Arabidopsis* Na+/H+ Antiporters NHX1 and NHX2 Control Vacuolar pH and K+ Homeostasis to Regulate Growth, Flower Development, and Reproduction [C][W]

Elias Bassil,[a] Hiromi Tajima,[a] Yin-Chih Liang,[a] Masa-aki Ohto,[a] Koichiro Ushijima,[b] Ryohei Nakano,[b] Tomoya Esumi,[a] Ardian Coku,[a] Mark Belmonte,[c] and Eduardo Blumwald[a,1]

[a] Department of Plant Sciences, University of California, Davis, California 95616
[b] Department of Agriculture, Okayama University, Okayama 700-8530, Japan
[c] Department of Biological Sciences, University of Manitoba, Winnipeg, Manitoba R3T 2N2, Canada

Intracellular Na+/H+ (NHX) antiporters have important roles in cellular pH and Na+, K+ homeostasis. The six *Arabidopsis thaliana* intracellular NHX members are divided into two groups, endosomal (NHX5 and NHX6) and vacuolar (NHX1 to NHX4). Of the vacuolar members, NHX1 has been characterized functionally, but the remaining members have largely unknown roles. Using reverse genetics, we show that, unlike the single knockouts *nhx1* or *nhx2,* the double knockout *nhx1 nhx2* had significantly reduced growth, smaller cells, shorter hypocotyls in etiolated seedlings and abnormal stamens in mature flowers. Filaments of *nhx1 nhx2* did not elongate and lacked the ability to dehisce and release pollen, resulting in a near lack of silique formation. Pollen viability and germination was not affected. Quantification of vacuolar pH and intravacuolar K+ concentrations indicated that *nhx1 nhx2* vacuoles were more acidic and accumulated only 30% of the wild-type K+ concentration, highlighting the roles of NHX1 and NHX2 in mediating vacuolar K+/H+ exchange. Growth under added Na+, but not K+, partly rescued the flower and growth phenotypes. Our results demonstrate the roles of NHX1 and NHX2 in regulating intravacuolar K+ and pH, which are essential to cell expansion and flower development.

INTRODUCTION

Ion homeostasis and the regulation of cellular pH are associated with every aspect of the biology of the cell. The concerted action of H+-translocating enzymes (H+-pumps) and cation/H+ exchangers are vital to establish and maintain optimal ion and pH gradients, which are essential for cell function and plant development (Martinoia et al., 2007; Amtmann and Leigh, 2010). Intracellular Na+/H+ antiporters (NHXs) are integral membrane proteins residing in the plasma membrane (Shi et al., 2000) endosomal compartments (Rodriguez-Rosales et al., 2008; Bassil et al., 2011), and vacuoles (Apse et al., 1999; Yokoi et al., 2002; Apse and Blumwald, 2007; Hamaji et al., 2009; Leidi et al., 2010). They belong to the monovalent cation/proton antiporter (CPA1) family of transporters (Maser et al., 2001). In plants, NHX antiporters catalyze the electroneutral exchange of Na+ and/or K+ for H+ by using the electrochemical H+ gradients generated by the (H+)–ATPases (in the plasma membrane) and the (H+)–ATPase and (H+)–PPase (in the vacuole) to direct either the movement of Na+ or K+ out of the cell or the luminal movement of Na+ or K+ into the vacuoles and intracellular organelles. The *NHX* gene family of *Arabidopsis thaliana* includes a class of six intracellular NHX-type antiporters, which are classified into two groups (Brett et al., 2005a; Pardo et al., 2006; Rodriguez-Rosales et al., 2009). Group I contains NHX1 to NHX4 and localizes to vacuoles, whereas group II contains NHX5 and NHX6 and localizes to endosomal compartments (Bassil et al., 2011). Several functions have been associated with plant NHX transporters, including the regulation of flower coloration (Yamaguchi et al., 2001; Ohnishi et al., 2005; Yoshida et al., 2009), the regulation of cellular K+ homeostasis (Venema et al., 2003; Pardo et al., 2006; Apse and Blumwald, 2007; Leidi et al., 2010), cell expansion (Apse et al., 2003; Bassil et al., 2011), vesicular trafficking and protein targeting (Bowers et al., 2000; Brett et al., 2005b; Bassil et al., 2011), and salt tolerance (Apse et al., 1999; Hernandez et al., 2009; Bassil et al., 2011). NHX1 was shown to be required for seedling establishment and leaf development, especially in the formation of large epidermal cells (Apse et al., 2003). Recently, NHX5 and NHX6 were shown to be localized in the Golgi and *trans*-Golgi network and to function in the trafficking of endosomal cargo to the vacuole, in salt stress, and in cell expansion (Bassil et al., 2011). However, the roles of the remaining members of the vacuolar group, NHX2, NHX3, and NHX4, in growth and development remain largely unknown. To comprehend the concerted role of all intracellular NHXs, an effort to generate and characterize multiple knockout lines of *Arabidopsis NHX1* to *NHX6* was initiated.

Although we have considerable information about the molecular and biochemical networks acting during plant growth and

development, we have little knowledge of how cells regulate the transport of solutes and their intracellular pH. Ions (K^+ in particular) and pH gradients have a great effect on the regulation of cell volume and the trafficking of membrane vesicles and their protein cargo between the different cellular compartments (Blumwald, 1987; Pardo et al., 2006; Bassil et al., 2011). These processes are essential for plant growth, development, and the response to environmental changes.

NHX-type cation/H^+ antiporters are critical players in cell expansion. To understand the concerted role of intracellular *Arabidopsis* NHXs on cell expansion, we initiated the characterization of the growth and development of *NHX1* and *NHX2* knockout lines. We show that *NHX1* and *NHX2* function together to control cell expansion in vegetative tissues and male reproductive organs and are required for normal flower development and set. We link flower developmental processes to altered vacuolar pH and K^+ homeostasis and argue that NHX1 and NHX2 mediate K^+/H^+ exchange to accumulate K^+ in the vacuole, a critical step for cell expansion and growth, especially in rapidly expanding cells.

RESULTS

At the organ level, the expression of *NHX1* and *NHX2* indicated that both genes are expressed ubiquitously, including roots, rosette leaves, stems, flowers, and siliques (see Supplemental Figure 1 online). The level of expression of *NHX1* was significantly higher than that of *NHX2* in all organs examined, and *NHX2* expression levels were similar to that of other *NHX* members (Bassil et al., 2011). The nearly ubiquitous expression of *NHX1* was also confirmed in publicly available expression data (http://bbc.botany.utoronto.ca/efp/cgi-bin/efpWeb.cgi) as wells as previously published work (Yokoi et al., 2002; Aharon et al., 2003; Apse et al., 2003).

NHX1 and NHX2 Colocalize to the Vacuole

To assess the localization of NHX1 and NHX2 and their possible vacuolar colocalization, we generated plants expressing C-terminal translational fusion reporter constructs with *NHX1* fused with green fluorescent protein (*GFP*), or *NHX2* fused with yellow fluorescent protein (*YFP*) or red fluorescent protein (*RFP*), driven by either the *Ubiquitin-10* (*Ub10*) or *35S* promoters. The growth of the transgenic reporter lines was indistinguishable from that of the wild-type plants, indicating that the fusion proteins did not adversely affect the growth of the transgenic plants. In *35S-NHX2-YFP* plants, the fluorescence signals in roots and root tips localized to vacuolar membranes (Figure 1; see Supplemental Figure 2 online). The vacuolar localization was clearly indicated by the nuclei seen outside the fluorescent boundary delineated by the NHX2-associated YFP signal (arrows in Figure 1A). Transvacuolar cytoplasmic strands were also clearly evident in root cells, which further supported the NHX2-YFP vacuolar association. Observation of *35S-NHX1-GFP* reporter plants resulted in a poor and inconsistent GFP signal that was often observed within the vacuolar lumen and endosomal bodies in all lines examined (see Supplemental Figure 2 online). To circumvent possible problems associated with overexpression or nonstable

expression caused by the *35S* promoter, *NHX1-GFP* was expressed under the control of the *Ub10* promoter, which enabled a milder, more stable expression of downstream genes (Grefen et al., 2010). Transient transformation of *Ub10-NHX1-GFP* in *Arabidopsis* seedlings resulted in a GFP signal associated with vacuolar membranes and transvacuolar strands (Figure 1B; see Supplemental Movie 1 online). Furthermore, plasmolysis of root cells, induced by the addition of 1 M mannitol, caused a clear recession of the tonoplast and the YFP and GFP signals, supporting the vacuolar localization of NHX1 and NHX2 (see Supplemental Figure 2 online). To determine whether NHX1 and NHX2 colocalize, *Ub10-NHX1-GFP* and *35S-NHX2-RFP* were transiently coexpressed in *Arabidopsis* seedlings. As shown in Figures 1C to 1E, NHX1-GFP and NHX2-RFP were highly colocalized to vacuolar membranes in cells expressing both transgenes. We also tested whether NHX1 colocalized with another vacuolar membrane protein by transiently expressing *Ub10-NHX1-GFP* in stable reporter lines of *VAMP711-RFP,* a R-SNARE of the tonoplast (Uemura et al., 2004). As expected, NHX1-GFP colocalized extensively with VAMP711 (Figures 1F to 1H).

nhx1 nhx2 Double Knockout Phenotypes

To investigate *NHX1* and *NHX2* functions, we used a reverse genetic approach to generate knockouts from available T-DNA insertion lines. Two independent knockout mutants using different T-DNA insertion lines for each gene were identified. Single knockouts, designated as *nhx1-1*, *nhx1-2*, *nhx2-1*, and *nhx2-3* (see Methods), were genotyped and backcrossed twice before their subsequent use in crosses to generate the independent double knockout lines *nhx1-1 nhx2-1*, *nhx1-2 nhx2-1*, and *nhx1-2 nhx2-3* (see Supplemental Figure 3 online). Lack of expression of full-length *NHX1* and *NHX2* in all knockouts was confirmed with RT-PCR (see Supplemental Figure 3 online). Experiments using the double knockout lines produced identical results; therefore, unless otherwise noted, results reported from here on are those obtained with the line *nhx1-1 nhx2-1*.

The single knockout *nhx1* displayed reduced growth compared with the wild type (Columbia ecotype [Col-0]), similar to that reported previously in *nhx1* in the Wassilewskija ecotype background (Apse et al., 2003). However, *nhx2* did not show any obvious growth phenotypes or developmental defects when grown either in soil (Figure 2A) or on plates (see below). By contrast, the double knockout *nhx1 nhx2* displayed a significant reduction in growth (Figure 2). Rosette leaf size and inflorescence height were markedly smaller than either the wild type or the single knockouts. Cross sections through leaf margins indicated that *nhx1 nhx2* cells were significantly smaller than comparable wild-type leaf cells (Figure 2B). *nhx1 nhx2* leaf tissue remained highly organized with no apparent cell-type disruptions. To confirm the *nhx1 nhx2* phenotypes, we complemented *nhx1 nhx2* with functional copies of both genes. Transformation of *nhx1 nhx2* with either *35S-NHX1-GFP* or 35S-*NHX2-YFP* reverted the growth phenotype to the wild type (Figure 2C), thereby demonstrating that the *nhx1 nhx2* phenotypes were caused by disruption of *NHX1* and *NHX2*. In addition, C-terminal tagging of NHX1 and NHX2 did not affect the function of either protein.
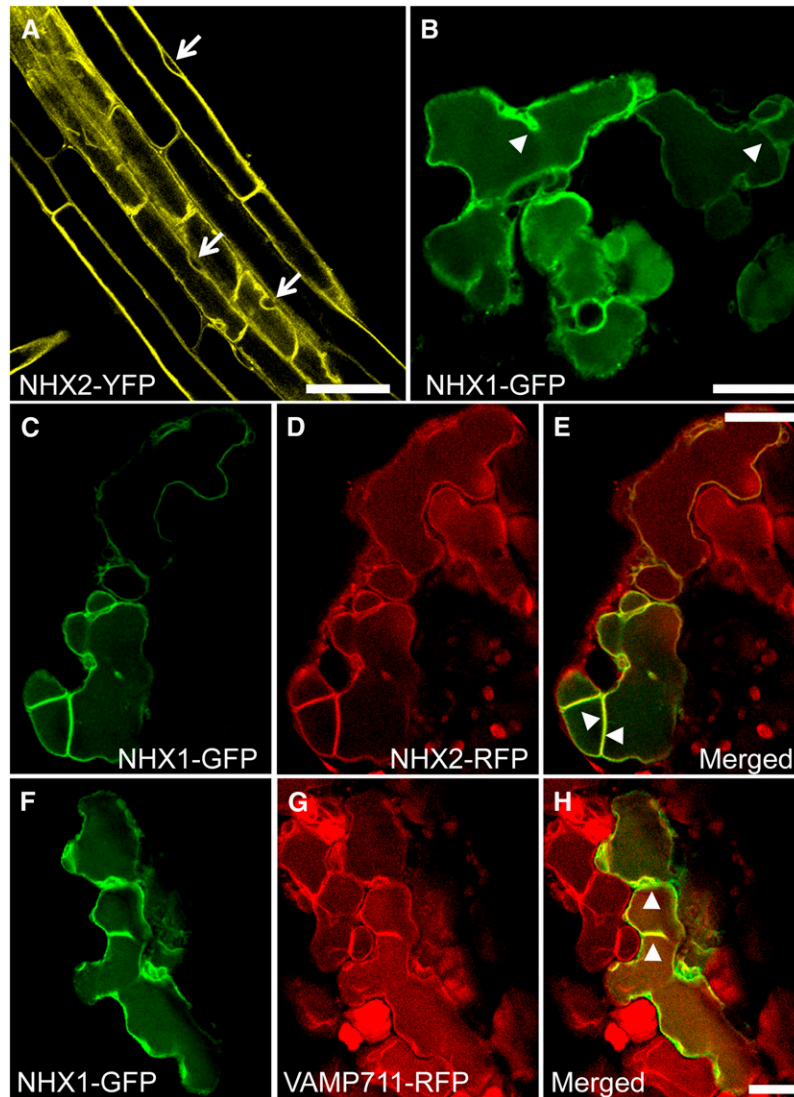
Figure 1. Subcellular Localization of NHX1 and NHX2.

(A) NHX2-associated YFP fluorescence in mature root cells of stably transformed plants expressing *35S-NHX2-YFP*. Arrows point to nuclei.
(B) Transient expression of *Ub10-NHX1-GFP* in *Arabidopsis* cotyledons.
(C) to **(E)** Transient coexpression of *Ub10-NHX1-GFP* and *35S-NHX2-RFP* in *Arabidopsis* cotyledons.
(F) to **(H)** Transient expression of *Ub10-NHX1-GFP* in the *Ub10-VAMP711-RFP* background.
(C) and **(F)** are GFP images; **(D)** and **(G)** are RFP images; **(E)** and **(H)** are merged images. Arrowheads in **(B)**, **(E)**, and **(H)** point to the tonoplast and transvacuolar cytoplasmic strands.
Bar in **(A)** = 50 mm; bars in **(B)** to **(H)** = 20 mm.

Stamens of *nhx1 nhx2* Lack Filament Elongation and Anther Dehiscence

nhx1 nhx2 plants displayed significant phenotypes in their reproductive organs. *nhx1 nhx2* flowers developed a low number of siliques, which contained few or no seeds (Figure 2D; see arrows). At the same developmental stage, *nhx1 nhx2* flowers were significantly shorter and narrower than the wild-type flowers (Figures 3A to 3C). A closer examination of flower

anatomy revealed at least two distinct developmental changes associated with stamens. First, mature *nhx1 nhx2* stamens had markedly shorter filaments that did not extend far enough to position the anthers at the height of the stigma (Figures 3B [arrows] and 3D), as is typically seen in the wild-type flowers. Quantitative measurements of filament lengths indicated that, in *nhx1 nhx2* flowers, both short and long filaments were reduced in length (Figure 3D). A comparison of longitudinal sections of filaments revealed that *nhx1 nhx2* filament cells
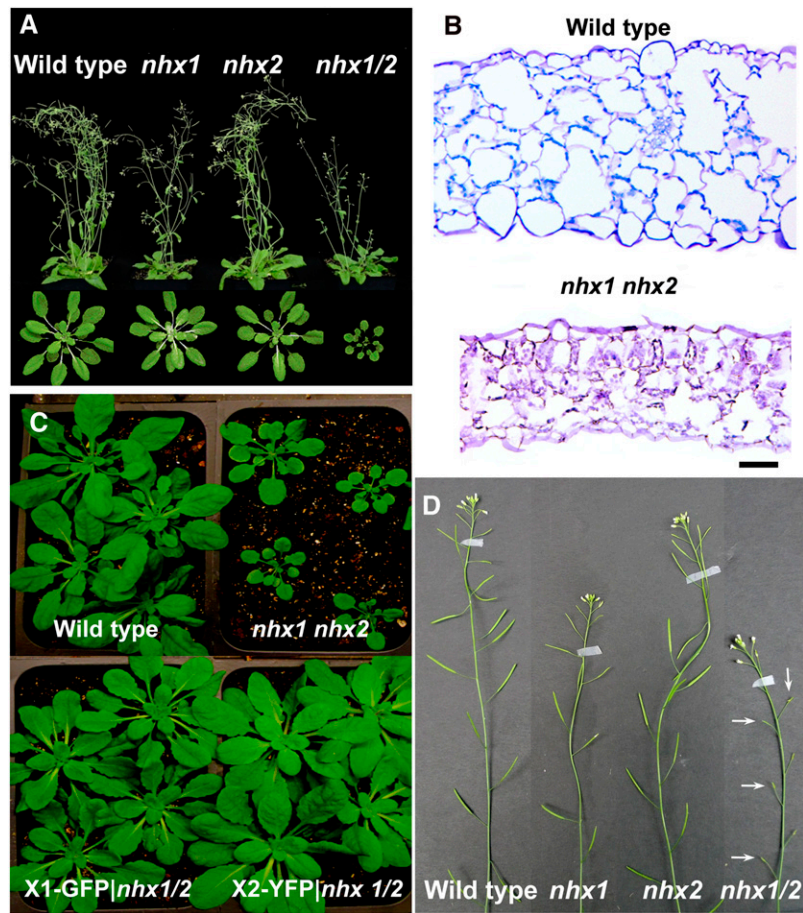
Figure 2. Growth and Development of the Single and Double Knockouts of *NHX1* and *NHX2*.

(A) Four-week-old plants grown under 16-h days **(Top)**, and 5-week-old plants grown under 8-h days **(Bottom)**.

(B) Cross section through the margin of a 4-week-old wild-type leaf **(Top)** and comparable *nhx1 nhx2* knockout leaf **(Bottom)**. Sections were stained with toluidine blue O.

(C) The *nhx1 nhx2* growth phenotype was rescued by transformation with either *35S-NHX1-GFP* or *35S-NHX2-YFP*. The wild type and *nhx1 nhx2* are included for comparison. Representative images of 4-week-old T1 transformants are shown.

(D) Inflorescence stalks of wild-type, *nhx1*, *nhx2*, and *nhx1 nhx2* plants. Note the lack of siliques in *nhx1 nhx2* (arrows).

Bar in **(B)** = 30 μm.

were only 55% the length and 60% the width of the wild-type filament cells (Figures 3E to 3G). The second stamen phenotype was that *nhx1 nhx2* anthers did not dehisce at the same frequency seen in the wild-type anthers (Figures 3B and 3C [insets]). Scoring of anthers from 40 *nhx1 nhx2* plants (~80 anthers) indicated that only 3% showed normal anther dehiscence. Cross sections of anthers showed that, in a high proportion of *nhx1 nhx2* anthers, the stomium (St in Figures 3H and 3I) did not rupture sufficiently to release pollen from individual anther locules (Figures 3H and 3I). When anther dehiscence did occur it was not sufficient to release and expose the majority of pollen. Therefore, *nhx1 nhx2* anthers lacked the characteristic yellowish color typical of anthers after dehiscence and remained the distinctive color of immature anthers (i.e., off-white) (Figures 3A and 3B [insets]). Eventually

nhx1 nhx2 flowers senesced without setting, and inflorescences of *nhx1 nhx2* did not form siliques (Figure 2B). A comparison of flower anatomy, the lack of anther dehiscence, and filament elongation in *nhx1 nhx2* are shown in the scanning electron micrographs of Figure 4.

To test specific expression of *NHX1* and *NHX2* in floral organs, we used *NHX1* and *NHX2* promoters to drive β-glucuronidase (*GUS*) expression in transgenic plants (see Supplemental Figure 4 online). GUS analysis indicated that the expression of *NHX1* was abundant in most flower organs (see Supplemental Figure 4A online) but was low in nonelongated filaments and immature anthers (see Supplemental Figure 4B online) and was highly expressed in elongated filaments (see Supplemental Figure 4C online). On the other hand, *NHX2* was highly expressed in anthers and pollen. These results might suggest
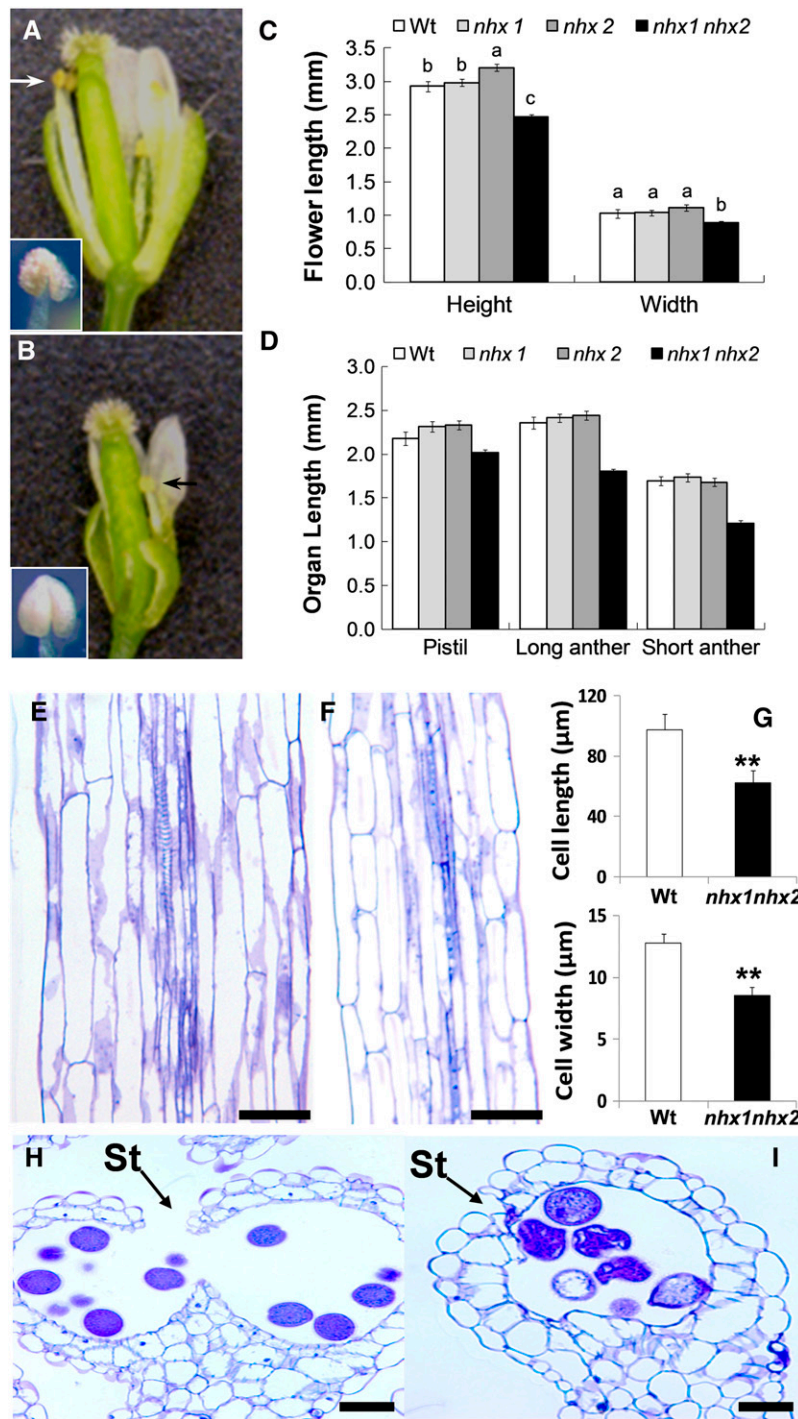
Figure 3. Stamens of the Double Knockout *nhx1 nhx2* Have Reduced Filament Elongation and Anther Dehiscence.

(A) Dissected wild-type flower showing normal filaments and anthers.
(B) Dissected *nhx1 nhx2* flower showing the short filament (arrows) and nondehiscent anther (inset) phenotypes.
(C) Quantification of whole flower size and **(D)** floral organ size in single and double knockouts of *NHX1* and *NHX2*. Wt, wild type.
(E) Longitudinal section of mature wild-type filament.
(F) Longitudinal section of mature *nhx1 nhx2* filament.
(G) Comparison of filament cell length and width.
(H) Cross section of a mature wild-type dehiscent anther with a ruptured stomium (St).
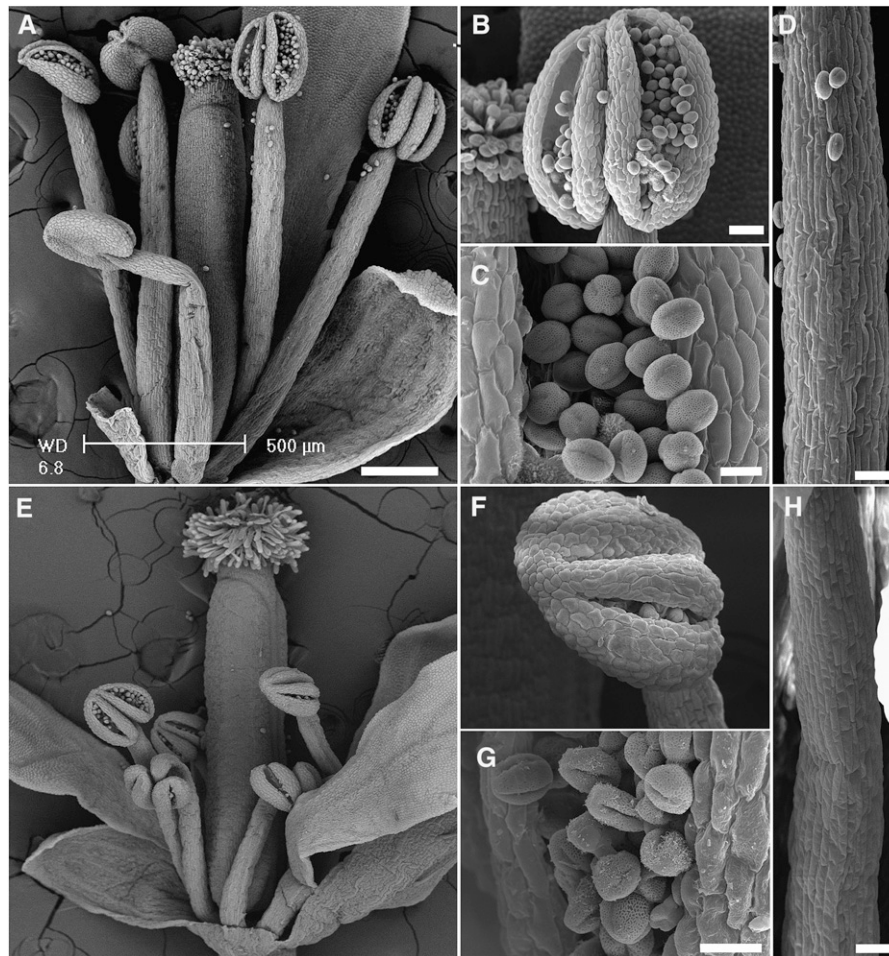
Figure 4. Scanning Electron Micrographs Comparing the Anatomy of the Wild-Type and *nhx1 nhx2* Flowers.

(A) to **(D)** Flowers and organs of the wild type.
(E) to **(F)** Flowers and organs of *nhx1 nhx2*.
(A) and **(E)** Whole flowers; **(B)** and **(F)** dehiscent anthers; **(C)** and **(G)** pollen grains; **(D)** and **(H)** filaments.
Bars in **(A)** and **(E)** = 200 μm; bars in **(B)**, **(F)**, **(D)**, and **(H)** = 50 μm; bars in **(C)** and **(G)** = 10 μm.

developmental-specific expression patterns for *NHX1* and *NHX2* and explain the flower phenotype that was observed in *nhx1 nhx2* but not in either *nhx1* or *nhx2* single knockouts. In addition, promoter GUS analysis indicated that *NHX1* was expressed throughout seedlings in all organs, whereas *NHX2* was expressed, albeit to a lesser extent, in root and shoot meristems and seedling vasculature (see Supplemental Figure 4 online).

Pollen Viability and Germination Were Not Affected in *nhx1 nhx2* Plants

The expression of *NHX1* and *NHX2* seen in pollen (see Supplemental Figure 4 online) prompted us to investigate whether pollen germination and viability were affected in *nhx1 nhx2* plants. For viability and germination experiments, approximately twice the number of *nhx1 nhx2* flowers were needed to obtain

Figure 3. (continued).

(I) Cross section of a mature *nhx1 nhx2* anther showing the lack of stomium rupture.
Different letters in **(C)** and **(D)** indicate significant difference using Tukey LSD test (P ≤ 0.05). Values in **(G)** represent the mean ± SD (*n* = 10). ** indicate significant difference between genotypes (P ≤ 0.001 and P ≤ 0.01, respectively; Student's *t* test).
Bars in **(E)**, **(F)**, **(H)**, and **(I)** = 30 μm.
[See online article for color version of this figure.]

similar amounts of pollen as were obtained from the wild type, probably because of the poor anther dehiscence in *nhx1 nhx2*. Pollen viability was examined by hydrating pollen on solidified gelatin and staining with 4′,6-diamidino-2-phenylindole (DAPI) (Alandete-Saez et al., 2008). No differences were detected in the rate or extent of pollen hydration between the wild type and *nhx1 nhx2* (Figure 5) or in pollen development, because DAPI staining of grains revealed that *nhx1 nhx2* had three nuclei (i.e., pollen mitosis I and II occurred normally) (Figures 5B and 5D). Pollen germination in *nhx1 nhx2* did not differ significantly from the wild type (Figure 5E). To determine which gametophyte was responsible for the *nhx1 nhx2* phenotype, reciprocal crosses were performed between the wild type and *nhx1 nhx2*. When the wild type was used as the female and *nhx1 nhx2* was used as a pollen donor (Wt/KO in Figures 5F and 5G), no effect on flower set was seen, and only a minor but nonsignificant reduction in silique length was observed compared with the wild-type control. These results suggest that *nhx1 nhx2* pollen tubes grew normally in vivo. However, when the wild type was used as the pollen donor to pollinate *nhx1 nhx2* emasculated plants (i.e., KO/Wt), only 74% of the flowers set, and the silique length was significantly shorter compared with Wt/KO or Wt/Wt controls. When *nhx1*

nhx2 was self-pollinated (KO/KO), only 49% of flowers set, and silique length was only marginally lower compared with KO/Wt crosses (Figures 5F and 5G). These results suggest that the lack of flower set and silique formation in *nhx1 nhx2* might not be due to lack of pollen viability or germination. In addition to the stamen abnormalities discussed above, the impaired growth of the *nhx1 nhx2* female gametophyte should be considered.

The Presence of NaCl in the Growth Medium Reduced *nhx1 nhx2* Flower and Growth Phenotypes

To gain additional insight into the role of *NHX1* and *NHX2* in vegetative and reproductive growth, *nhx1 nhx2* plants were grown under different salinity conditions. A clear difference was observed between *nhx1 nhx2* plants grown in the presence and absence of 100 mM NaCl (Figures 6A and 6B). Unlike *nhx1 nhx2* grown in the absence of salt, *nhx1 nhx2* plants grown on 100 mM NaCl were able to produce siliques (Figures 6A and 6B). A closer examination of the flowers revealed that in salt-grown *nhx1 nhx2* plants, the filaments were fully elongated, and the anthers dehisced (Figures 6C to 6E). A quantification of flower set indicated that *nhx1 nhx2* flower set increased from 8% in nonsaline conditions to 57% on 100 mM NaCl (Figure 6F). These
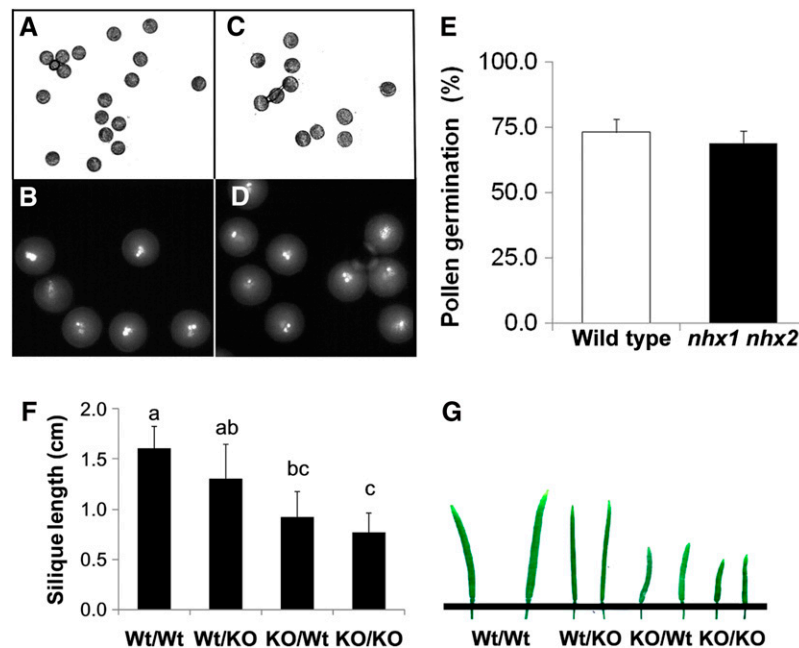

Figure 5. Pollen Viability and Germination Is Not Significantly Affected in the *nhx1 nhx2* Double Knockout.

Wild-type **(A)** and **(B)** and *nhx1 nhx2* **(C)** and **(D)** pollen after 2 h of hydration on gelatin-coated slides.
(B) and **(D)** DAPI staining of hydrated pollen, indicating tricellular pollen.
(E) Pollen germination was assessed by scoring germinated pollen grains from an aliquot of pollen incubated in germination media (see Methods) on microscope slides observed within defined areas. A pollen grain was considered germinated when the length of the pollen tube exceeded the diameter of the pollen grain. Approximately 100 pollen grains were counted in each of 25 defined areas. Values are the mean $\pm$ SD ($n = 25$).
(F) Quantification of silique length obtained from reciprocal crosses between wild type (wt) and *nhx1 nhx2* (KO) (designated as female/male). For each cross, 20 siliques were measured. Values represent the mean $\pm$ SD ($n = 20$). Similar letters indicate no significant difference (P $\leq$ 0.05) using Tukey LSD test.
(G) Picture representation of the data in **(F)**.
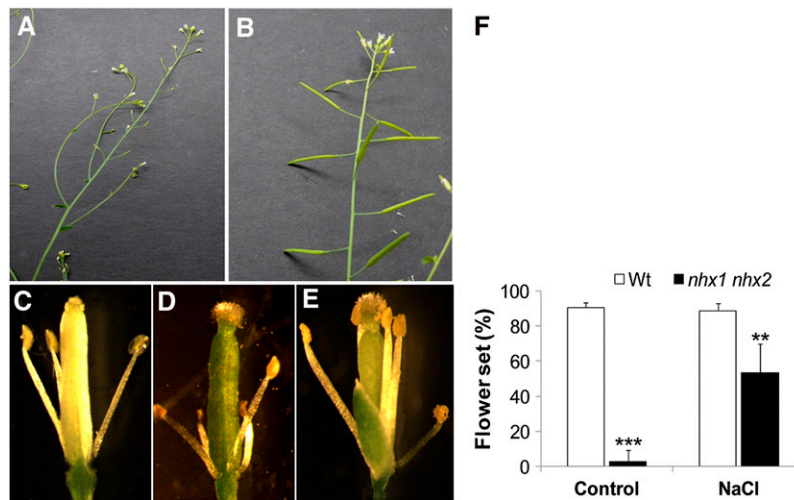[See online article for color version of this figure.]

Figure 6. The *nhx1 nhx2* Flower Phenotype Is Rescued When Plants Are Grown in High Salt.

Plants were grown in soil under short days (8 h light) for 4 weeks and then irrigated with 50 mM NaCl followed by 100 mM NaCl 2 d later. An additional 25 mM NaCl was included once a week with irrigation. At 5 weeks, the plants were switched to long days (16 h light) to induce flowering. At 7 weeks, flowers were examined.

(A) *nhx1 nhx2* inflorescence from plants grown under control conditions showing the characteristic lack of developed siliques.

(B) Inflorescence of *nhx1 nhx2* when grown in soil supplemented with 100 mM NaCl.

(C) Dissected wild-type flower showing fully elongated and dehiscent anthers.

(D) Dissected *nhx1 nhx2* flower from plants grown without added salt showing short filaments and nondehiscent anthers.

(E) Dissected *nhx1 nhx2* flower from plants grown under 100 mM NaCl showing fully elongated and dehiscent anthers.

(F) Comparison of flower set (%) in wild-type (Wt) and *nhx1 nhx2* plants grown in the presence and absence of 100 mM NaCl. The primary inflorescence of each of 10 plants was used for counts. ** and ***, significant difference between genotypes (P $\leq$ 0.01 and P $\leq$ 0.001, respectively). Values are the mean $\pm$ SD (*n* = 25 flowers). The experiment was repeated twice.

[See online article for color version of this figure.]

results would suggest that Na$^+$ ions partially substituted the lack of K$^+$ accumulation in filament cell vacuoles.

Given the roles of NHX-type transporters in Na$^+$ and K$^+$ homeostasis (Pardo et al., 2006; Apse and Blumwald, 2007), we assessed whether the growth of *nhx1 nhx2* was affected by varying the concentrations of K$^+$ and Na$^+$ in the growth media. The growth of the wild-type plants in media supplemented with either 30 mM of Na$^+$ or K$^+$ or equimolar concentrations of both did not differ significantly (Figure 7). The biomass of *nhx1 nhx2*, however, increased at 30 mM Na$^+$ compared with *nhx1 nhx2* grown in control media (i.e., 1 mM Na$^+$ and 1 mM K$^+$) but remained significantly lower than the biomass of the wild-type plants grown at 30 mM Na$^+$. Moreover, in the presence of 30 mM K$^+$, the growth *of nhx1 nhx2* decreased by 30% compared with that of *nhx1 nhx2* plants grown in control media, and was only 5% the weight of the wild-type plants (Figure 7I). A close-up of *nhx1 nhx2* plants in the 30 mM K$^+$ treatment indicated that the rosette formed a tight ball composed of curled leaves that lacked leaf and petiole expansion compared with *nhx1 nhx2* in the high Na$^+$ or control treatments (Figure 7J). Plants also displayed severe yellowing and necrosis of some leaves. In addition, in the presence of 30 mM K$^+$, *nhx1 nhx2* roots were profusely curled, forming concentric circles and a partial loss of growth toward the axis of gravity (Figure 7K). Under an equimolar concentration of Na$^+$ plus K$^+$ (30 mM each), the weight of *nhx1 nhx2* plants

increased only moderately, and although it was higher than that of seedlings grown in control media, it remained significantly lower than that of the wild type (Figure 7I). The negative effects of K$^+$ on growth of *nhx1 nhx2* plants were also observed in experiments that used KNO$_3$ instead of KCl as a salt source. Identical results were also obtained when dry weights were used for the same analysis. These results indicate that moderate amounts of Na$^+$ in the media improved growth of *nhx1 nhx2*, whereas an equimolar amount of K$^+$ was unfavorable to growth.

In wild-type plants, leaf K$^+$ and Na$^+$ contents increased with increased K$^+$ and Na$^+$ in the media (see Supplemental Figure 5 online). The leaf concentrations of K$^+$ were higher than those of Na$^+$ in all treatments and genotypes tested. Furthermore, the wild-type leaf K$^+$ content was higher than that of *nhx1 nhx2* leaves from all treatments. Leaf K$^+$ contents were also influenced by the presence of Na$^+$ in the media and differed substantially between the wild type and *nhx1 nhx2*. For example, in the wild type, there was a small but significant increase in leaf K$^+$ content in plants grown in 30 mM Na$^+$ compared with plants grown in control media. In 30 mM Na$^+$–grown *nhx1 nhx2* plants, leaf K$^+$ content was lower than of control-grown plants. In *nhx1 nhx2*, leaf Na$^+$ contents did not differ in media with added K$^+$. The differential leaf K$^+$ content was also reflected by the K$^+$:Na$^+$ ratio, which was halved in *nhx1 nhx2* plants grown in all treatments (Figure 7J). The Na$^+$:K$^+$ ratio was also significantly higher in *nhx1*
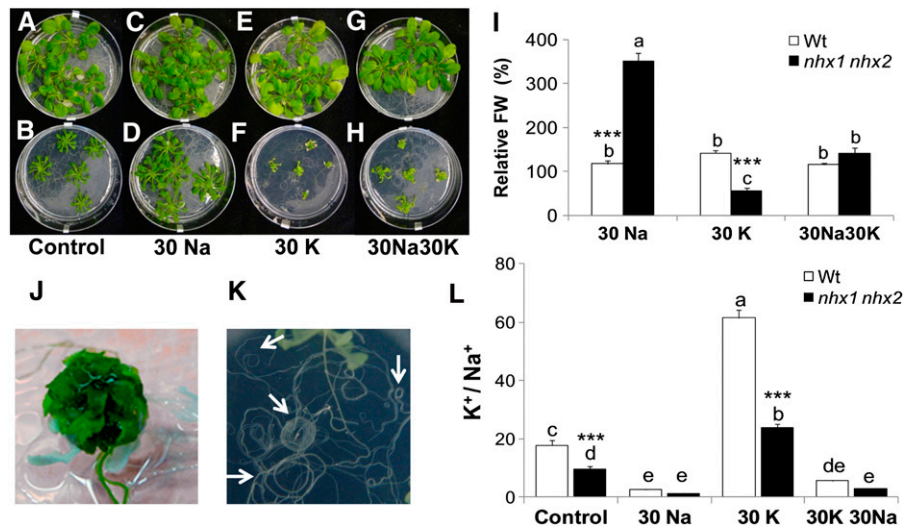
Figure 7. Growth and Ion Content of the *nhx1 nhx2* Double Knockout Depends on K$^+$ and Na$^+$ in Media.

Four-week-old wild-type plants **(A)**, **(C)**, **(E)**, and **(G)** and *nhx1 nhx2* **(B)**, **(D)**, **(F)**, and **(H)** were grown in modified Spalding media containing:
(A) and **(B)** 1 mM K$^+$ and 1 mM Na$^+$ (control), **(C)** and **(D)** 1 mM K$^+$ and 30 mM Na$^+$ (30Na), **(E)** and **(F)** 30 mM K$^+$ and 1 mM Na$^+$ (30K), and **(G)** and **(H)** 30 mM K$^+$ and 30 mM Na$^+$ (30K30Na).
(I) Relative shoot fresh weight (FW) (compared with control media of each genotype) of plants shown in **(A)** to **(H)**. Values are the mean ± SD (*n* = 25 plants). Similar letters indicate no significant difference (P < 0.05 using Tukey LSD test. ***, significant difference between genotypes (P ≤ 0.01; Student's *t* test). Wt, wild type.
(J) Close-up image of *nhx1 nhx2* shoots grown in 30 mM K$^+$.
(K) Close-up image of *nhx1 nhx2* showing severe root curling in 30 mM K$^+$ but not 30 mM Na$^+$. Arrows point to regions of profuse root curling.
(L) Ratio of leaf K$^+$ and Na$^+$ content. Values are the mean ± SD (*n* = 5). Similar letters indicate no significant difference (P < 0.05) using Tukey LSD test. ***, significant difference between genotypes (P ≤ 0.001, respectively).

nhx2 than in the wild type at both 30 mM Na$^+$ and 30 mM Na$^+$ plus 30 mM K$^+$ treatments. Collectively, these data indicate that the ability of *nhx1 nhx2* plants to accumulate K$^+$ in favor of Na$^+$ was compromised and that these plants were not able to adjust their K$^+$ content when challenged with Na$^+$, as seen in the wild-type plants.

Etiolation of *nhx1 nhx2* Seedlings Is Cation Dependent

We reasoned that a good experimental system to test the role(s) of NHX1 and NHX2 in rapid cell expansion would be the etiolation response of dark-grown seedlings, because etiolated seedlings are amenable to physiological and cellular measurements of pH and K$^+$ homeostasis. Furthermore, the rapid elongation of hypocotyls in etiolated seedlings closely parallels the elongation of anther filaments during flower development. When grown on solidified media in the dark, *nhx1 nhx2* etiolated seedlings displayed significantly shorter hypocotyls and longer roots than the wild-type seedlings (see Supplemental Figure 6A online). Etiolated seedlings grown on increasing concentrations of K$^+$ exhibited a progressively stronger phenotype (i.e., significantly shorter hypocotyls and longer roots than control-grown *nhx1 nhx2*). Interestingly, when K$^+$ concentrations in the media were 10 mM or more, roots of *nhx1 nhx2* grew by curling away from the direction of gravity, forming concentric circles of winding roots, which was probably caused by uneven expansion of epidermal

cells (see Supplemental Figure 6 online). Similar to the response of long-term plant growth experiments (Figure 7), hypocotyls of *nhx1 nhx2* seedlings grown in 30 mM Na$^+$ elongated more than those of *nhx1 nhx2* in control media and were not significantly different in length from the wild-type hypocotyls. The root response, however, did not recover under increased Na$^+$ as it did in hypocotyls. The consistent phenotype and response of etiolated seedlings allowed for a reliable experimental system to perform additional cellular measurements (as described below).

NHX1 and NHX2 Regulate Vacuolar pH and K$^+$ Homeostasis

To assess the roles of NHX1 and NHX2 in pH regulation, we used the ratiometric fluorescein-based pH sensitive dye, 2′,7′-bis-(2-carboxyethyl)-5-(and-6)-carboxyfluorescein (BCECF) in an imaging-based approach to measure vacuolar pH in vivo. Ratiometric dyes have the distinct advantage of not being significantly affected by dye loading, cell size, or tissue morphology, unlike other nonratiometric dyes. The membrane-permeant BCECF-acetoxymethyl (AM) derivative readily loads into vacuoles of intact root cells (Swanson et al., 1998; Krebs et al., 2010). pH values were calculated from fluorescence ratios of confocal images using an in situ calibration curve (see Supplemental Figure 7 online). Because of the imaging nature of the technique, it was possible to measure vacuolar pH along the entire root zone of seedlings from root tip to hypocotyl. Vacuolar
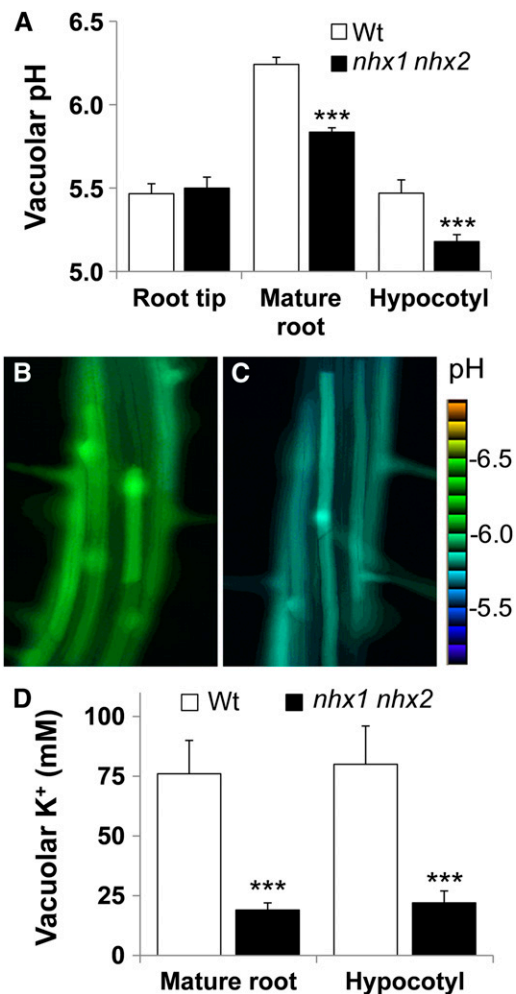
Figure 8. Vacuoles of *nhx1 nhx2* in Root and Hypocotyl Cells Are More Acidic and Contain Less K+ than Comparable Wild-Type Cells.

(A) Vacuolar pH in roots and hypocotyl of 4-d etiolated seedlings. Wt, wild type.

(B) Ratio images of wild-type or **(C)** *nhx1 nhx2* cells of the mature root zone, indicating lower pH in *nhx1 nhx2*. The Intensity Modulated Display mode of MetaMorph (Molecular Devices) was used to generate the ratio images and accompanying scale bar. pH was calculated from the fluorescence ratio of confocal images collected in roots and hypocotyls cells of seedlings loaded with the pH-sensitive dye BCECF-AM. After background correction, an integrated pixel intensity value (ImageJ 1.43, National Institutes of Health) was calculated in emission (535 to 550 nm) images after excitation with 488 nm and divided by those acquired when excited by 458 nm to obtain ratio images. Ratio images were used to calculate pH from a calibration curve (see Supplemental Figure 7 online) generated as described in Methods. Error bars are the SD of 35 measurements (i.e., ratio images) representing approximately 15 to 20 cells in at least 10 different seedlings. The experiment was repeated six times. Particular care was taken to use images from similar regions of the root, because a comparison of pH along the root indicated that vacuolar pH is not uniform across all cells along the seedling root (mature root and root tip pH values).

(D) The vacuolar K+ concentration is lower in *nhx1 nhx2* seedlings than the wild type. Vacuolar K+ was measured as described for BCECF-AM except the dye PBFI-AM was used (see Methods). Values are the mean ± SD (*n* = 30). ***, significant difference (P ≤ 0.001; Student's *t* test).

pH in root tip cells (i.e., cells that were not fully expanded, as seen in Supplemental Figure 7B online), was lower (pH 5.5) than in the mature zone (pH 6.3 to 5.8) but was similar to that in hypocotyl cells (pH 5.5 to 5.2) (Figure 8A). In root tip cells, no significant difference between the wild-type and *nhx1 nhx2* vacuolar pH was observed. However, in cells of the mature root zone and the hypocotyl, vacuolar pH was nearly 0.5 and 0.35 pH units lower, respectively, in *nhx1 nhx2* (Figure 8A). Figures 8B and 8C show the typical ratio images showing the BCECF-associated vacuolar fluorescence in mature root zone cells from the wild type and *nhx1 nhx2*.

We next measured vacuolar K+ with a similar imaging approach (to that of pH discussed above), using the ratiometric K+-sensitive dye potassium-binding benzofuran isophthalate acetoxymethyl ester (PBFI-AM) (Halperin and Lynch, 2003). We found that a longer incubation time was needed to load the AM form of the dye into the vacuole of cortical and hypocotyl cells than was reported for loading into the cytosol of root hair cells (Halperin and Lynch, 2003). The vacuolar localization of the dye was confirmed using confocal images of root tip cells, in which it is easy to discern vacuole from cytosol (see Supplemental Figure 7B online). Under our experimental conditions, the vacuolar K+ concentrations of root cells of the mature zone as well as hypocotyl cells were ~75 mM (±12 mM). In *nhx1 nhx2*, however, K+ concentrations were significantly lower and were near 20 mM (±4 mM). Both a lower vacuolar pH and lower K+ concentration in *nhx1 nhx2* are consistent with the notion of tonoplast-localized NHX1 and NHX2 mediating vacuolar K+/H+ exchange.

DISCUSSION

The in planta localization of NHX1 and NHX2 provides key information on their functions. In *Arabidopsis* cell cultures, Hamaji et al. (2009) immunolocalized NHX1 to vacuoles, and Yokoi et al. (2002) transiently expressed NHX2 in onion epidermal cells to show vacuolar localization, whereas Apse et al. (1999) used membrane fractionation to localize NHX1 to the tonoplast. Here we show that NHX1 and NHX2 colocalize to the vacuole. We also observed that in some reporter lines, the NHX1-GFP signal was associated with punctate and motile endosomal bodies in addition to labeling of the vacuole. Although this might be an artifact of the 35S promoter-driver expression, it is interesting to note that Hamaji et al. (2009) also observed similarly sized vesicles that were immunolabeled with NHX1 in salt-treated plants. They suggested that NHX1 may have roles in salt stress, either through tonoplast augmentation via vesicular trafficking, or that NHX1 in an endosomal or prevacuolar compartment may be critical for salt stress, as suggested by Hernandez et al. (2009). A role of NHX1 in vesicular trafficking was also inferred from microarray analysis of *nhx1* transcripts, in which many vesicular trafficking genes were differentially expressed (Sottosanto et al., 2004).

Using a reverse genetic approach, we characterized the growth and development phenotypes of several T-DNA insertion lines of *NHX1* and *NHX2*. In the Col-0 background, *nhx1* knockout plants displayed a similar reduction in growth as described previously for *nhx1* in the WS background (Apse et al., 2003). In

the former study, we showed that epidermal cell expansion, especially that of large highly vacuolated cells, was significantly reduced in the single knockout *nhx1*, which caused a mild but significant decrease in overall plant growth (Apse et al., 2003). Here we show that the single knockout *nhx2* did not exhibit any obvious growth or developmental phenotypes. However, the double knockout *nhx1 nhx2* had a more severe reduction in vegetative growth than that of *nhx1*, and this reduction was associated with a substantial decrease in cell size rather than defects in tissue organization. Our data support the notion that *NHX1* and *NHX2* might function in a partially redundant manner to control cell expansion.

Roles of NHX1 and NHX2 in Stamen Development and Function

The double knockout *nhx1 nhx2* also displayed two distinct floral organ developmental phenotypes, which were not seen in either of the single knockouts, *nhx1* or *nhx2*. The first phenotype was that filaments did not elongate far enough to place anthers at the height of the stigma. Longitudinal sections of filaments indicated that individual filament cells in *nhx1 nhx2* were 70% the length of the wild-type cells. The second phenotype was that *nhx1 nhx2* anther dehiscence occurred in only 7% of flowers. Together, both phenotypes likely lead to the observed lack of flower set and silique formation in *nhx1 nhx2*. Given the role of NHX1 in mediating vacuolar K^+/H^+ exchange (Blumwald and Poole, 1985; Zhang and Blumwald, 2001; Venema et al., 2002; Yamaguchi et al., 2003; Leidi et al., 2010) and the proposed specific role of K^+ in filament extension (Heslop-Harrison and Heslop-Harrison, 1996), it is plausible that the reduced cell expansion observed in *nhx1 nhx2* filaments might result from a lack of sufficient K^+ accumulation in vacuoles of filament cells, which is necessary for osmotic driven cell expansion.

Anther dehiscence is a coordinated process that depends on the active hydration and subsequent dehydration of select anther tissues, including the endothecium and epidermal cells. Hydration directs a turgor-induced force that ultimately ruptures a weakened stomium and causes the opening of the anther locules to expose and release pollen (Scott et al., 2004). Water movement within anthers has been suggested to occur as a consequence of localized accumulation of ions and K^+ in particular (Matsui et al., 2000; Rehman and Yun, 2006). A transfer of K^+ from the anther locule to pollen grains has also been postulated to cause swelling of pollen grains, which contributes to stomium rupture (Wilson et al., 2011). It is worth noting that we also observed that a significant number of *nhx1 nhx2* pollen grains shrunk (Figures 3I and 4G), perhaps because of insufficient swelling.

Here, the stamen phenotypes correlated with filament- and anther-specific expression of NHX1 and NHX2. These observations are supported by available microarray data (Zimmermann et al., 2004) as well as by previous results (Apse et al., 2003). These data also suggest that NHX1 and NHX2 might have specific roles in pollen development and/or pollen tube growth. Recently, it was also shown that two cation/proton exchangers (CHXs) are needed to guide pollen tubes toward the ovule (Lu et al., 2011). However, pollen viability, germination, and recipro-

cal crossing experiments between the wild-type and *nhx1 nhx2* plants suggested that pollen development and its ability to germinate in vitro and in vivo might not be significantly affected in *nhx1 nhx2* plants. Thus, it is possible that the roles of CHXs and NHX1 and NHX2 are complementary and that CHXs have both broad and specialized roles in development. Collectively, our data point to a developmentally coordinated role in which NHX1 and NHX2 regulate K^+ homeostasis in stamens, and this homeostasis enables filament elongation and anther dehiscence to occur.

Interestingly, when soil-grown *nhx1 nhx2* plants were watered with solutions containing 100 mM NaCl, filament elongation and flower set was restored, along with a concomitant and significant increase in silique formation (Figure 6). These results suggest that other vacuolar transporters, possibly NHX3, NHX4, and/or CHXs, are mediating H^+-driven Na^+ uptake into vacuoles, allowing for osmotic-driven vacuolar expansion to elongate the filament and bypass the specific requirement of K^+ accumulation in filament cells.

Regulation of Vacuolar pH and K+ Homeostasis to Control Cell Expansion

The lack of cell expansion and tissue elongation in *nhx1 nhx2* plants was not limited to leaves and filaments but was also observed in hypocotyls of etiolated seedlings, in which *nhx1 nhx2* hypocotyls were shorter than the wild type. Using seedlings, we measured vacuolar pH and K^+ content in hypocotyl and root cell vacuoles and found that in *nhx1 nhx2,* vacuolar pH was more acidic, and K^+ content was only 30% of that in the wild-type cells. These differences were only observed in highly vacuolated cells of the mature root zone and the hypocotyl and not in the nonvacuolated cells of the root tip, suggesting a close relationship between NHX1, NHX2, vacuolar K^+ and pH homeostasis, and cell size. Our values for vacuolar pH (5.5) and K^+ (75 mM in the wild type) were similar to other reported values obtained using ^{31}P NMR **(**Martinez and Lauchli, 1993**)** ion-selective microelectrodes (Walker et al., 1996; Carden et al., 2003; Leidi et al., 2010) and fluorescent dyes (Swanson et al., 1998; Halperin and Lynch, 2003; Krebs et al., 2010). Assuming a cytosolic concentration of 100 mM K^+, a tonoplast membrane potential of 30 mV, and steady state with the cytosol, the vacuolar K^+ concentration would be $\sim$20 mM and similar to the vacuolar K^+ content we measured in *nhx1 nhx2* cells. A more acidic pH and significantly lower K^+ content of *nhx1 nhx2* are consistent with the localization and biochemical function of NHX transporters at the tonoplast.

In the single knockout *nhx1,* Apse et al. (2003) measured a reduction in K^+/H^+ and Na^+/H^+ exchange and, because of this and the reduced cell expansion phenotype of *nhx1*, proposed that under normal physiological conditions, NHX1 regulates vacuolar K^+ and/or pH to control cell expansion. Using NHX1-overexpressing tomatoes, Leidi et al. (2010) concluded that NHX1 overexpression led to increased vacuolar K^+ accumulation at the expense of cytosolic K^+ depletion, which was correlated with early K^+ deficiency symptoms, upregulation of *HAK5* expression, and greater K^+ uptake compared with the wild type, despite the measurement of higher tissue K^+ content in

transgenic plants. Our results closely mirror the findings of Leidi et al. (2010) and essentially point to a similar function of NHX1 and NHX2. Under normal growth conditions (i.e., low Na^+ concentrations), these two exchangers primarily mediate K^+/H^+ exchange, as supported by earlier findings (Zhang and Blumwald, 2001; Apse et al., 2003).

Most cellular K^+ is located within the vacuole, where it serves as an osmoticum to drive turgor, but significant amounts (80 to 100 mM) also exist in the cytosol, where it is critical for protein function and stability and as an enzyme cofactor (Leigh and Jones, 1984; Amtmann and Leigh, 2010). The vacuolar K^+ pool is a main supplier of cytosolic K^+, because under varying external K^+ concentrations, cytosolic K^+ is tightly maintained, whereas the vacuolar K^+ pool fluctuates with K^+ supply and tissue content (Walker et al., 1996). The data of Walker et al. strongly implied that cytosolic K^+ might be maintained in part by exchange with the vacuole, a role that can be satisfied in part by NHX-type antiporters. At the typical tonoplast membrane potential ($\sim$30 mV, positive inside), transport of K^+ would occur against its potential, which suggests that it must be energized (Martinoia et al., 2000). Our data support this notion. When grown on K^+-supplemented media (30 mM), nhx1 nhx2 growth was adversely affected compared with that in normal K^+ (1 mM). Given that the electrochemical potential of K^+ favors uptake into the cell as well as the lack in K^+ vacuolar accumulation, we reason that a high supply of K^+ was deleterious to nhx1 nhx2 growth, probably because K^+ was accumulating to toxic levels in the cytosol. Although there is significant information on the consequences of limiting K^+ uptake at the plasma membrane, little is known about the possible consequences of increasing cytosolic K^+ by limiting vacuolar K^+ sequestration. In other words, little is known about cellular responses to elevated cytosolic K^+. This is probably because when plants are exposed to high external K^+ concentrations, changes in cytosolic K^+ are efficiently modulated by the compartmentation of K^+ into vacuoles (Walker et al., 1996; Leigh, 2001). In this respect, given the low exchange of K^+ at the tonoplast in nhx1 nhx2, these plants could serve as a useful tool to study the cellular effects of shifts in cytosolic K^+ homeostasis. The adverse response of nhx1 nhx2 plants to high external K^+ raises interesting questions about cellular K^+ homeostasis and feedback control between vacuole, cytosol, and the extracellular medium. The toxic effects of such relatively low (30 mM) K^+ concentration on the nhx1 nhx2 seedlings might also suggest indirect effects on other cellular functions. For example, cytosolic K^+ could induce the dephosphorylation of the plasma membrane (H^+)–ATPase, downregulating its activity with the concomitant decrease in the transmembrane electrochemical H^+ gradient (Buch-Pedersen et al., 2006). These aspects are beyond the scope of this study and require further investigation.

The growth of nhx1 nhx2 plants increased significantly in the presence of moderate amounts of Na^+ (30 mM), supporting the notion that Na^+ uptake into the vacuole does not depend solely on NHX1 and NHX2 activities, and that Na^+ is transported into the vacuole through other transporters. Na^+ likely substituted in part for the lack of K^+ accumulation in vacuoles, where it induced cell expansion by increasing the osmotic potential and turgor that was probably insufficient in nonsalinized nhx1 nhx2. It is well known that at low K^+ conditions, Na^+ can partly substitute for K^+

in the vacuole and can therefore positively affect growth (Bartels and Sunkar, 2005). At low concentrations (<30 mM NaCl in the case of Arabidosis), Na^+ was beneficial to growth, because it probably served as a metabolically cheap osmoticum (Bartels and Sunkar, 2005). Nevertheless, Na^+ did not replace the plant's K^+ requirements, because the vegetative and reproductive phenotype of nhx1 nhx2 when grown under added Na^+ were not completely rescued.

Increased vacuolar acidification in nhx1 nhx2 would also result in changes in the electrical potential differences across the tonoplast (i.e., depolarization), which could affect the vacuolar H^+-pump activity and the activities of other transporters, in particular gated ion channels (Pantoja et al., 1992). A critical role of NHX antiporters in pH regulation is best exemplified by their function in alkalinization of the vacuole during petal development and color transitions in Japanese morning glory (Ipomoea nil) (Yamaguchi et al., 2001; Ohnishi et al., 2005). In addition, NHX1 activity is regulated by a calmodulin-like protein at the C terminus in a Ca^{2+}- and pH-dependent manner. Binding of the calmodulin-like protein to NHX1 decreased the V_{max} for Na^+/H^+ exchange but not for K^+/H^+ exchange, thereby modulating H^+-coupled Na^+ or K^+ exchange (Yamaguchi et al., 2005). This regulation has important implications under salt stress, in which a low $Na^+:K^+$ ratio must be maintained in the cytosol. Given the lower vacuolar pH of nhx1 nhx2, it is possible that the regulation of NHX1 selectivity may be altered, influencing the differential response of nhx1 nhx2 plants to Na^+ versus K^+. Other roles of vacuolar pH, especially those associated with cell expansion, remain largely unknown but may be linked to vesicular trafficking and membrane fusion (Honsbein et al., 2011).

In summary, NHX1 and NHX2 are vacuolar proteins that control vacuolar pH and K^+ homeostasis. We provide evidence to support the role of NHX1 and NHX2 in mediating K^+/H^+ exchange. This exchange regulates cell expansion in rapidly elongating tissues, such as filaments and hypocotyls, and plays unique and specific roles in flower development.

METHODS

Plant Materials and Growth Conditions

Arabidopsis thaliana (Col-0) were grown in soil at 22°C under diurnal light conditions as specified below. For plate-grown plants, modified Murashige and Skoog media (Spalding et al., 1999), with 1% phytagel (Sigma-Aldrich), no Suc, and pH 5.7. 1 mM Na^+ was considered the control Na^+ concentration. For Na^+ and K^+ experiments, media were supplemented with KCl or NaCl as indicated in the figure legends. Plate-grown plants were incubated at 22°C for 12 h light and 12 h dark. For flower analysis, the wild-type and nhx1 nhx2 plants were grown in soil under short days (8 h light), and at 4 weeks, were irrigated with 50 mM NaCl followed by 100 mM NaCl 2 d later. An additional 25 mM NaCl was included once a week with irrigation. At 5 weeks, the plants were switched to long days (16 h light) to induce flowering.

T-DNA insertion mutants (Col-0) (http://signal.salk.edu/cgi-bin/tdnaexpress) for NHX1 were nhx1-1 (SALK_34001) and nhx1-2 (SALK_065623) and for NHX2 were nhx2-1 (SALK_036114) and nhx2-3 (SALK_084844). Positions of T-DNA insertion sites are shown in Supplemental Figure 3 online. RT-PCR confirmed no DNA amplification with allele-specific primers from knockout-derived cDNA. All single knockouts were backcrossed with Col-0 wild-type plants twice, and corresponding lines with single T-DNA insertions were selected by DNA gel blot hybridization using the left border

sequence as the probe. Primer sequences for the confirmation of homozygous T-DNA insertions are listed in Supplemental Table 1 online.

Plasmid Construction and Plant Transformation

All of the constructs in this study were generated using the Gateway system (Invitrogen). cDNAs of *NHX1* and *NHX2* (without stop codons) were cloned into pDONR207 (Invitrogen) to generate entry vectors (pDONR207-NHX1, pDONR207-NHX2) and recombined into pEarleyGate103 for GFP fusion and pEarleyGate101 for YFP fusion (Earley et al., 2006). The constructs were introduced into *Arabidopsis* Col-0 plants expressing translational fusion proteins, and into *nhx1-1 nhx2-1* for complementation by *Agrobacterium tumefaciens* (GV3101) using the floral dipping method (Clough and Bent, 1998). The *Ub10-NHX1-GFP* construct was generated using Multisite Gateway method (Invitrogen). 634 bp of Ubiquitin-10 promoter was cloned from pNIGEL07 (Geldner et al., 2009) into pDONRP4P1r (Invitrogen) to generate pDONRL4R1-UBQ10pro as a first fragment entry vector. The pDONRL4R1-UBQ10pro was recombined with the entry vectors pDONR207-NHX1 and pENR2-F-L3 into pB7m34GW destination vector (Karimi et al., 2007). For the *35S-NHX2-RFP* construct, pDONR207-NHX2 was recombined into pH7RWG2 (Karimi et al., 2007). The *Ub10-NHX1-GFP* and the *35S-NHX2-RFP* were introduced into *A. tumefaciens* strain EHA105. Those constructs were transiently expressed in cotyledons of the wild-type and VAMP711-RFP *Arabidopsis* seedlings (Marion et al., 2008). A list of primers is included in Supplemental Table 1 online.

Pollen Viability and Germination

Flowers of the wild type and *nhx1 nhx2* were harvested in the morning and used to dust pollen on 2.5% gelatin (from porcine skin; Sigma-Aldrich) solidified on glass plates. To assay pollen viability, several drops of water containing 1 μM DAPI were added to the gelatin pad. Pollen germination was modified from the protocol of (Boavida and McCormick, 2007). Pollen from 50 wild-type flowers and 100 *nhx1 nhx2* flowers were collected in a 1.5-mL tube with liquid germination medium (0.01% H_3BO_3, 5 mM $CaCl_2$, 5 mM KCl, 1 mM $MgSO_4$, 5 mM Tris-MES [pH 7.5], 10% Suc) and vortexed briefly. Pollen was pelleted for 1 min at 13,000 rpm, resuspended in 250 μL fresh pollen germination medium, and transferred to small glass vials with their screw caps loosely attached. Pollen was germinated at 22°C in light for 6 h, without agitation. 50-μL aliquots were used to assess percent germination from defined areas of slides. Pollen germination medium was always made fresh from stock solutions. For reciprocal crosses, flowers were emasculated at night 18 to 20 h before cross-pollination. Given the slower development of *nhx1 nhx2* flowers, and to ensure that all flowers were at the same developmental stage, *nhx1 nhx2* flowers used for crosses were ~20 h older than the wild-type flowers.

Histological Analysis

Preparation of plant tissues was performed as previously reported (Bassil et al., 2011). Briefly, tissue was fixed in formalin–acetic acid–alcohol, under vacuum, rinsed, and dehydrated in a graded series of ethanol before being mixed with xylenes and paraffin and sectioned. Serial sections were stained with periodic acid–Schiff for total carbohydrates and were counterstained with amido black 10B for protein or toluidine blue O for general histological organization.

Fluorescence and Light Microscopy

Fluorescence microscopy was performed using a Leica confocal laser-scanning microscope (DM RXE 6 TCS-SP2 AOBS) equipped with a 63× water immersion objective. The excitation wavelength was 488 nm for GFP and 594 nm for RFP, and emission was 500 to 535 nm for GFP and 600 to 660 for RFP. To avoid crosstalk between fluorescence channels, sequential scanning was used when necessary. Images were processed with ImageJ (http://rsbweb.nih.gov/ij/).

Electron Microscopy

Mature flowers were partly dissected to expose floral organs before fixation (2.5% paraformaldehyde, 2.0% glutaraldehyde in 0.08 M sodium phosphate buffer, pH 7.2) under vacuum (1 h) and were rinsed with 0.1 M sodium phosphate buffer. Tissue was then dehydrated in ascending concentrations of ethyl alcohol (30, 50, 70, 95, and 100%), then dried in a critical point dryer, mounted onto aluminum stubs, and coated with gold. Flowers were viewed with a scanning electron microscope using 20 kV (Philips XL30 TMP; FEI) at the University of California, Davis (Electron Microscopy Laboratory, Department of Pathology and Laboratory Medicine, School of Medicine).

Measurement of Vacuolar K^{+} and pH

Vacuolar pH was measured using the pH-sensitive dye BCECF-AM in root and hypocotyls cells of 5-d-old seedlings grown on vertical plates. Dye loading was performed as described by Krebs et al. (2010) with minor modifications. Briefly, seedlings were incubated in 1/10 Murashige and Skoog liquid medium (0.5% Suc, 10 mM MES, pH 5.7) containing 10 μM BCECF-AM 0.02% pluronic F-127 (Molecular Probes) for 1 h in darkness at 22°C and were washed twice before microscopy. Dye fluorescence images were collected using a Leica confocal laser-scanning microscope (DM RXE 6 TCS-SP2 AOBS) equipped with a 20× objective after excitation with 458 and 488 nm. Single emission between 525 and 550 nm was collected for each excitation wavelength. Images were collected from root tip cells, mature root cells of the elongation zone, and hypocotyls cells. After background correction, the integrated pixel intensity was measured for both the 458 nm-excited images and the 488 nm-excited images, and ratios were calculated (ImageJ v1.43; National Institutes of Health). Fluorescence ratio values were used to calculate the pH from a calibration curve. For pH calibration, seedlings were equilibrated 15 min before observation in equilibration buffer containing 50 mM BTP-HEPES or MES (pH 5.0 to 7.4) and 50 mM ammonium acetate. For each ratio value, 10 images from each of 25 seedlings were measured, and the experiment was repeated at least five times.

For determination of vacuolar K^{+}, the ratiometric dye PBFI-AM (Molecular Probes) procedure (Halperin and Lynch, 2003) was used with slight modifications. PBFI-AM was loaded into 5-d-old seedlings as described for BCECF-AM above, except that 20 μM and 18 h of loading were used. Images above 500 nm emission were collected when roots and hypocotyls were excited with 360 nm and 380 nm, respectively, using an Hg lamp source fitted to a Leica DMRE running MetaMorph v7.1 (Molecular Devices). In situ calibration of vacuolar K^{+} was performed by incubating dye-loaded tissue with 2 μM gramicidin in dye-loading buffer and concentrations of KCl (0 to 100 mM) to generate a standard curve of fluorescence ratio (Halperin and Lynch, 2003). There is an inherent difficulty in buffering K^{+} near zero when performing in vivo calibrations, but this was not a significant limitation, because all measured values fell within the calibration range (i.e., ratios corresponding to 15 mM and above). Images were corrected for background fluorescence as described for BCECF-AM.

Leaf Ion Contents

The samples were weighed and digested in ~3 mL of 3:1 HNO_3:H_2O_2 for 24 h. An aliquot of the digest was diluted 30-fold with 3% HNO_3 and was

measured with inductively coupled plasma atomic emission spectroscopy.

RNA Preparation and Expression Analysis

Total RNA was extracted from rosette leaves using RNeasy Mini kit (Qiagen) with six biological replicates, treated with DNaseI, and subsequently purified with RNeasy RNA purification column (Qiagen). First-strand cDNA was synthesized from 1 μg of total RNA with the QuantiTect Reverse Transcription Kit (Qiagen). Primer Express (Applied Biosystem, Life Technologies) was used to design primers. Quantitative PCR (qPCR) was performed on the StepOnePlus (Applied Biosystems) using SYBR GREEN (Bio–Rad). The reaction volume included 2 μL template, 0.3 μL of reverse primer, 0.3 μL of forward primer, 7.5 μL SYBR Green Master Mix, and 4.9 μL RNA-free water (total 15 μL). qPCR was performed as follows: 95°C for 10 min followed by 40 cycles of 95°C for 30 s and 60°C for 30 s. The cycle threshold (CT) $2^{-\Delta\Delta CT}$ method (Livak and Schmittgen, 2001) was used to determine the relative mRNA using PP2A as an internal reference, because PP2A was previously found to express similarly in all genotypes and organs examined here (Bassil et al., 2011). Primer sequences for RT-PCR and qPCR are listed in Supplemental Table 1 online.

Accession Numbers

Sequence data from this article can be found in the Arabidopsis Genome Initiative database under the following accession numbers: NHX1 (At5g27150) and NHX2 (At3g05030).

Supplemental Data

The following materials are available in the online version of this article.

Supplemental Figure 1. Tissue-Specific Expression of *NHX1* and *NHX2*.

Supplemental Figure 2. Subcellular Localization of NHX1 and NHX2.

Supplemental Figure 3. T-DNA Insertion Mutants of *NHX1* and *NHX2*.

Supplemental Figure 4. Organ-Specific Expression of *NHX1* and *NHX2* in Inflorescence Clusters and Flowers.

Supplemental Figure 5. Concentrations of Na+ and K+ in Rosette Leaves of *nhx1 nhx2*.

Supplemental Figure 6. Etiolation Response of Germinating *nhx1 nhx2* Seedlings Depends on Ion Content of Media.

Supplemental Figure 7. pH Calibration Curve of BCECF-AM Dye-Loaded Roots.

Supplemental Table 1. List of Primers Used in This Study.

Supplemental Movie 1. Movie of Figure 1.

Supplemental Movie Legends. Vacuolar Colocalization of NHX1-GFP and NHX2-RFP.

AUTHOR CONTRIBUTIONS

E. Bassil and E. Blumwald designed the research. E. Bassil, H.T., Y.-C.L., M.O., T.E., K.U., R.N., A.C., and M.B. performed the research. E. Bassil and E. Blumwald wrote the article.

REFERENCES

Aharon, G.S., Apse, M.P., Duan, S., Hua, X., and Blumwald, E. (2003). Characterization of a family of vacuolar Na+/H+ antiporters in *Arabidopsis thaliana*. Plant Soil **253:** 245–256.

Alandete-Saez, M., Ron, M., and McCormick, S. (2008). GEX3, expressed in the male gametophyte and in the egg cell of *Arabidopsis thaliana*, is essential for micropylar pollen tube guidance and plays a role during early embryogenesis. Molecular Plant **1:** 586–598.

Amtmann, A., and Leigh, R. (2010). Ion homeostasis. In Abiotic Stress Adaptation in Plants, A. Pareek, S.K. Sopory, and H.J. Bohnert, eds (Dordrecht, The Netherlands: Springer), pp. 245–262.

Apse, M.P., and Blumwald, E. (2007). Na+ transport in plants. FEBS Lett. **581:** 2247–2254.

Apse, M.P., Sottosanto, J.B., and Blumwald, E. (2003). Vacuolar cation/H+ exchange, ion homeostasis, and leaf development are altered in a T-DNA insertional mutant of AtNHX1, the *Arabidopsis* vacuolar Na+/H+ antiporter. Plant J. **36:** 229–239.

Apse, M.P., Aharon, G.S., Snedden, W.A., and Blumwald, E. (1999). Salt tolerance conferred by overexpression of a vacuolar Na+/H+ antiport in *Arabidopsis*. Science **285:** 1256–1258.

Bartels, D., and Sunkar, R. (2005). Drought and salt tolerance in plants. Crit. Rev. Plant Sci. **24:** 23–58.

Bassil, E., Ohto, M.A., Esumi, T., Tajima, H., Zhu, Z., Cagnac, O., Belmonte, M., Peleg, Z., Yamaguchi, T., and Blumwald, E. (2011). The *Arabidopsis* intracellular Na+/H+ antiporters NHX5 and NHX6 are endosome associated and necessary for plant growth and development. Plant Cell **23:** 224–239.

Blumwald, E. (1987). Tonoplast vescicles as a tool in the study of ion-transport at the plant vacuole. Physiol. Plant. **69:** 731–734.

Blumwald, E., and Poole, R.J. (1985). Na+/H+ antiport in isolated tonoplast vesicles from storage tissue of Beta vulgaris. Plant Physiol. **78:** 163–167.

Boavida, L.C., and McCormick, S. (2007). Temperature as a determinant factor for increased and reproducible in vitro pollen germination in *Arabidopsis thaliana*. Plant J. **52:** 570–582.

Bowers, K., Levi, B.P., Patel, F.I., and Stevens, T.H. (2000). The sodium/proton exchanger Nhx1p is required for endosomal protein trafficking in the yeast *Saccharomyces cerevisiae*. Mol. Biol. Cell **11:** 4277–4294.

Brett, C.L., Donowitz, M., and Rao, R. (2005a). Evolutionary origins of eukaryotic sodium/proton exchangers. Am. J. Physiol. Cell Physiol. **288:** C223–C239.

Brett, C.L., Tukaye, D.N., Mukherjee, S., and Rao, R.J. (2005b). The yeast endosomal Na+(K+)/H+ exchanger Nhx1 regulates cellular pH to control vesicle trafficking. Mol. Biol. Cell **16:** 1396–1405.

Buch-Pedersen, M.J., Rudashevskaya, E.L., Berner, T.S., Venema, K., and Palmgren, M.G. (2006). Potassium as an intrinsic uncoupler of the plasma membrane H+-ATPase. J. Biol. Chem. **281:** 38285–38292.

Carden, D.E., Walker, D.J., Flowers, T.J., and Miller, A.J. (2003). Single-cell measurements of the contributions of cytosolic Na+ and K+ to salt tolerance. Plant Physiol. **131:** 676–683.

Clough, S.J., and Bent, A.F. (1998). Floral dip: A simplified method for Agrobacterium-mediated transformation of *Arabidopsis thaliana*. Plant J. **16:** 735–743.

Earley, K.W., Haag, J.R., Pontes, O., Opper, K., Juehne, T., Song, K., and Pikaard, C.S. (2006). Gateway-compatible vectors for plant functional genomics and proteomics. Plant J. **45:** 616–629.

Geldner, N., Denervaud-Tendon, V., Hyman, D.L., Mayer, U., Stierhof, Y.D., and Chory, J. (2009). Rapid, combinatorial analysis of membrane compartments in intact plants with a multicolor marker set. Plant J. **59:** 169–178.

Grefen, C., Donald, N., Hashimoto, K., Kudla, J., Schumacher, K., and Blatt, M.R. (2010). A ubiquitin-10 promoter-based vector set for fluorescent protein tagging facilitates temporal stability and native protein distribution in transient and stable expression studies. Plant J. **64:** 355–365.

Halperin, S.J., and Lynch, J.P. (2003). Effects of salinity on cytosolic Na+ and K+ in root hairs of *Arabidopsis thaliana*: In vivo measurements using the fluorescent dyes SBFI and PBFI. J. Exp. Bot. **54:** 2035–2043.

Hamaji, K., et al. (2009). Dynamic aspects of ion accumulation by vesicle traffic under salt stress in Arabidopsis. Plant Cell Physiol. **50:** 2023–2033.

Hernandez, A., Jiang, X.Y., Cubero, B., Nieto, P.M., Bressan, R.A., Hasegawa, P.M., and Pardo, J.M. (2009). Mutants of the *Arabidopsis thaliana* cation/H+ antiporter AtNHX1 conferring increased salt tolerance in yeast. The endosome/prevacuolar compartment is a target for salt toxicity. J. Biol. Chem. **284:** 14276–14285.

Heslop-Harrison, Y., and Heslop-Harrison, J.S. (1996). Lodicule function and filament extension in the grasses: Potassium ion movement and tissue specialization. Ann. Bot. (Lond.) **77:** 573–582.

Honsbein, A., Blatt, M.R., and Grefen, C. (2011). A molecular framework for coupling cellular volume and osmotic solute transport control. J. Exp. Bot. **62:** 2363–2370.

Karimi, M., Bleys, A., Vanderhaeghen, R., and Hilson, P. (2007). Building blocks for plant gene assembly. Plant Physiol. **145:** 1183–1191.

Krebs, M., Beyhl, D., Gorlich, E., Al-Rasheid, K.A.S., Marten, I., Stierhof, Y.D., Hedrich, R., and Schumacher, K. (2010). *Arabidopsis* V-ATPase activity at the tonoplast is required for efficient nutrient storage but not for sodium accumulation. Proc. Natl. Acad. Sci. USA **107:** 3251–3256.

Leidi, E.O., Barragan, V., Rubio, L., El-Hamdaoui, A., Ruiz, M.T., Cubero, B., Fernandez, J.A., Bressan, R.A., Hasegawa, P.M., Quintero, F.J., and Pardo, J.M. (2010). The AtNHX1 exchanger mediates potassium compartmentation in vacuoles of transgenic tomato. Plant J. **61:** 495–506.

Leigh, R.A. (2001). Potassium homeostasis and membrane transport. J. Plant Nutr. Soil Sci. **164:** 193–198.

Leigh, R.A., and Jones, R.G.W. (1984). A hypothesis relating critical potassium concentrations for growth to the distribution and functions of this ion in the plant-cell. New Phytol. **97:** 1–13.

Livak, K.J., and Schmittgen, T.D. (2001). Analysis of relative gene expression data using real-time quantitative PCR and the 2(-Delta Delta C(T)) method. Methods **25:** 402–408.

Lu, Y., Chanroj, S., Zulkifli, L., Johnson, M.A., Uozumi, N., Cheung, A., and Sze, H. (2011). Pollen tubes lacking a pair of K+ transporters fail to target ovules in *Arabidopsis*. Plant Cell **23:** 81–93.

Marion, J., Bach, L., Bellec, Y., Meyer, C., Gissot, L., and Faure, J.D. (2008). Systematic analysis of protein subcellular localization and interaction using high-throughput transient transformation of *Arabidopsis* seedlings. Plant J. **56:** 169–179.

Martinez, V., and Lauchli, A. (1993). Effects of Ca2+ on the salt-stress response of barley roots as observed by in-vivo P-31-nuclear magnetic-resonance and in-vitro analysis. Planta **190:** 519–524.

Martinoia, E., Massonneau, A., and Frangne, N. (2000). Transport processes of solutes across the vacuolar membrane of higher plants. Plant Cell Physiol. **41:** 1175–1186.

Martinoia, E., Maeshima, M., and Neuhaus, H.E. (2007). Vacuolar transporters and their essential role in plant metabolism. J. Exp. Bot. **58:** 83–102.

Maser, P., et al. (2001). Phylogenetic relationships within cation transporter families of *Arabidopsis*. Plant Physiol. **126:** 1646–1667.

Matsui, T., Omasa, K., and Horie, T. (2000). High temperature at flowering inhibits swelling of pollen grains, a driving force for thecae dehiscence in rice (*Oryza sativa* L.). Plant Prod. Sci. **3:** 430–434.

Ohnishi, M., Fukada-Tanaka, S., Hoshino, A., Takada, J., Inagaki, Y., and Iida, S. (2005). Characterization of a novel Na+/H+ antiporter gene InNHX2 and comparison of InNHX2 with InNHX1, which is responsible for blue flower coloration by increasing the vacuolar pH in the Japanese morning glory. Plant Cell Physiol. **46:** 259–267.

Pantoja, O., Gelli, A., and Blumwald, E. (1992). Characterization of vacuolar malate and K+ channels under physiological conditions. Plant Physiol. **100:** 1137–1141.

Pardo, J.M., Cubero, B., Leidi, E.O., and Quintero, F.J. (2006). Alkali cation exchangers: Roles in cellular homeostasis and stress tolerance. J. Exp. Bot. **57:** 1181–1199.

Rehman, S., and Yun, S.J. (2006). Developmental regulation of K accumulation in pollen, anthers, and papillae: Are anther dehiscence, papillae hydration, and pollen swelling leading to pollination and fertilization in barley (*Hordeum vulgare* L.) regulated by changes in K concentration? J. Exp. Bot. **57:** 1315–1321.

Rodriguez-Rosales, M.P., Jiang, X.Y., Galvez, F.J., Aranda, M.N., Cubero, B., and Venema, K. (2008). Overexpression of the tomato K+/H+ antiporter LeNHX2 confers salt tolerance by improving potassium compartmentalization. New Phytol. **179:** 366–377.

Rodriguez-Rosales, M.P., Galvez, F.J., Huertas, R., Aranda, M.N., Baghour, M., Cagnac, O., and Venema, K. (2009). Plant NHX cation/proton antiporters. Plant Signal. Behav. **4:** 265–276.

Scott, R.J., Spielman, M., and Dickinson, H.G. (2004). Stamen structure and function. Plant Cell **16:** S46–S60.

Shi, H., Ishitani, M., Kim, C., and Zhu, J.-K. (2000). The *Arabidopsis thaliana* salt tolerance gene SOS1 encodes a putative Na+/H+ antiporter. Proc. Natl. Acad. Sci. USA **97:** 6896–6901.

Sottosanto, J.B., Gelli, A., and Blumwald, E. (2004). DNA array analyses of *Arabidopsis thaliana* lacking a vacuolar Na+/H+ antiporter: Impact of AtNHX1 on gene expression. Plant J. **40:** 752–771.

Spalding, E.P., Hirsch, R.E., Lewis, D.R., Qi, Z., Sussman, M.R., and Lewis, B.D. (1999). Potassium uptake supporting plant growth in the absence of AKT1 channel activity: Inhibition by ammonium and stimulation by sodium. J. Gen. Physiol. **113:** 909–918.

Swanson, S.J., Bethke, P.C., and Jones, R.L. (1998). Barley aleurone cells contain two types of vacuoles: Characterization of lytic organelles by use of fluorescent probes. Plant Cell **10:** 685–698.

Uemura, T., Ueda, T., Ohniwa, R.L., Nakano, A., Takeyasu, K., and Sato, M.H. (2004). Systematic analysis of SNARE molecules in *Arabidopsis*: Dissection of the post-Golgi network in plant cells. Cell Struct. Funct. **29:** 49–65.

Venema, K., Quintero, F.J., Pardo, J.M., and Donaire, J.P. (2002). The *Arabidopsis* Na+/H+ exchanger AtNHX1 catalyzes low affinity Na+ and K+ transport in reconstituted liposomes. J. Biol. Chem. **277:** 2413–2418.

Venema, K., Belver, A., Marin-Manzano, M.C., Rodriguez-Rosales, M.P., and Donaire, J.P. (2003). A novel intracellular K+/H+ antiporter related to Na+/H+ antiporters is important for K+ ion homeostasis in plants. J. Biol. Chem. **278:** 22453–22459.

Walker, D.J., Leigh, R.A., and Miller, A.J. (1996). Potassium homeostasis in vacuolate plant cells. Proc. Natl. Acad. Sci. USA **93:** 10510–10514.

Wilson, Z.A., Song, J., Taylor, B., and Yang, C. (2011). The final split: The regulation of anther dehiscence. J. Exp. Bot. **62:** 1633–1649.

Yamaguchi, T., Apse, M.P., Shi, H.Z., and Blumwald, E. (2003). Topological analysis of a plant vacuolar Na+/H+ antiporter reveals a luminal C terminus that regulates antiporter cation selectivity. Proc. Natl. Acad. Sci. USA **100:** 12510–12515.

Yamaguchi, T., Aharon, G.S., Sottosanto, J.B., and Blumwald, E. (2005). Vacuolar Na+/H+ antiporter cation selectivity is regulated by calmodulin from within the vacuole in a Ca2+- and pH-dependent manner. Proc. Natl. Acad. Sci. USA **102:** 16107–16112.

Yamaguchi, T., Fukada-Tanaka, S., Inagaki, Y., Saito, N., Yonekura-Sakakibara, K., Tanaka, Y., Kusumi, T., and Iida, S. (2001). Genes encoding the vacuolar Na+/H+ exchanger and flower coloration. Plant Cell Physiol. **42:** 451–461.

Yokoi, S., Quintero, F.J., Cubero, B., Ruiz, M.T., Bressan, R.A., Hasegawa, P.M., and Pardo, J.M. (2002). Differential expression and function of *Arabidopsis thaliana* NHX Na+/H+ antiporters in the salt stress response. Plant J. **30:** 529–539.

Yoshida, K., Miki, N., Momonoi, K., Kawachi, M., Katou, K., Okazaki, Y., Uozumi, N., Maeshima, M., and Kondo, T. (2009). Synchrony between flower opening and petal-color change from red to blue in morning glory, Ipomoea tricolor cv. Heavenly Blue. Proc. Jpn. Acad. Ser. B Phys. Biol. Sci. **85:** 187–197.

Zhang, H.X., and Blumwald, E. (2001). Transgenic salt-tolerant tomato plants accumulate salt in foliage but not in fruit. Nat. Biotechnol. **19:** 765–768.

Zimmermann, P., Hirsch-Hoffmann, M., Hennig, L., and Gruissem, W. (2004). GENEVESTIGATOR. Arabidopsis Microarray Database and Analysis Toolbox. Plant Physiol. **136:** 2621–2632.

The *Arabidopsis* Na$^+$/H$^+$ Antiporters NHX1 and NHX2 Control Vacuolar pH and K$^+$ Homeostasis to Regulate Growth, Flower Development, and Reproduction

Elias Bassil, Hiromi Tajima, Yin-Chih Liang, Masa-aki Ohto, Koichiro Ushijima, Ryohei Nakano,
Tomoya Esumi, Ardian Coku, Mark Belmonte and Eduardo Blumwald

Plant Cell 2011;23;3482-3497; originally published online September 27, 2011;
DOI 10.1105/tpc.111.089581

This information is current as of November 1, 2011